Accepted for publication in PASP

Sensitivity of a Ground-Based Infrared Interferometer for Aperture Synthesis Imaging

Tadashi Nakajima
National Astronomical Observatory, 2-21-1 Osawa, Mitaka, 181-8588, Japan;
tadashi.nakajima@nao.ac.jp

ABSTRACT

Sensitivity limits of ground-based infrared interferometers using aperture synthesis are presented. The motivation of this analysis is to compare an interferometer composed of multiple large telescopes and a single giant telescope with adaptive optics. In deriving these limits, perfect wavefront correction by adaptive optics and perfect cophasing by fringe tracking are assumed. We consider the case in which n beams are pairwise combined at $n(n-1)/2$ detectors (${}^nC_2$ interferometer) and the case in which all the n beams are combined at a single detector (${}^nC_n$ interferometer). Our analysis covers broadband observations by considering spectral dispersion of interference fringes. In the read noise limit, the ${}^nC_n$ interferometer with one dimensional baseline configuration is superior to the ${}^nC_2$ interferometer, while in the background limit, the advantage of the one-dimensional ${}^nC_n$ interferometer is small. As a case study, we compare the point-source sensitivities of interferometers composed of nine 10-m diameter telescopes and a 30-m diameter single telescope with adaptive optics between 1 and 10 μm for 10-σ detection in one hour. At J and H, the sensitivities of the interferometers are limited to 25 to 24 mag by read noise and OH airglow background, while that of the single telescope is limited to 28 to 26 mag by OH airglow background. Longward of 2 μm, the sensitivities of the interferometers and the single telescope are all limited by instrumental thermal background. At K, the sensitivities of the interferometers are around 23 mag, while that of the single telescope is 27 mag. At N, the sensitivities of the interferometers are around 10.7 mag, while that of the single telescope is 14.4 mag.

Subject headings: techniques: interferometric

1. Introduction

Fundamental limitations of optical and infrared aperture synthesis imaging had been an academic subject in which astronomers were not keenly interested. The analyses of sensitivities

are mathematically rather involved and they appeared in journals of optics (Prasad & Kulkarni (1989) (PK89), Nakajima & Matsuhara (2001) (NM01)) instead of those in astronomy. The analyses were academic partly because they dealt with ideal conditions in which atmospheric disturbances did not exist. Therefore their results were applicable only to space interferometers which were instruments in the distant future. They were also academic partly because optical and infrared interferometers were not considered as routinely used astronomical instruments unlike radio interferometers in radio astronomy.

However, as pointed out by Roddier & Ridgway (1999) (hereafter RR99), the situation has changed due to the completion of large ground-based telescopes with 8-10 m diameters and to the planning of next-generation giant telescopes with 30-100 m diameters. In the plans of the giant telescopes, they are all equipped with adaptive optics which deliver diffraction limited images. The giant telescopes are always useful as optical buckets. However for the purpose of high resolution imaging, it is not clear whether the synthesized images from an interferometric array of large telescopes or diffraction limited images of giant telescopes are superior. In terms of resolution, the interferometric array is obviously advantageous, but in terms of sensitivity or dynamic range the quantitative comparison is more complex. Optical/infrared interferometric arrays with small telescopes currently in operation or being built are dedicated to stellar astronomy. With the advent of an interferometric array composed of large telescopes, one essential question is whether interferometry finally has an impact on extragalactic astronomy. This question is directly related to the limiting magnitude.

The development of the fringe-tracking technique has enabled to cophase a number of telescopes and a ground-based interferometric array can be regarded as an ideal interferometer without atmospheric disturbances. Therefore the sensitivity analyses made for space interferometers in the past can now be applied to ground-based interferometers as well. Under these circumstances, it is worthwhile to highlight the results of previous analyses of optical and infrared synthesis imaging in an astronomical journal and apply them to ground-based interferometry composed of large telescopes.

RR99 pioneered the analysis of ground-based interferometry from the point of view of comparison with future giant telescopes. However their analysis is not of aperture synthesis and as we will show later that their results are not necessarily in agreement with ours. Although this paper mostly utilizes previously obtained formulae of signal-to-noise ratios (SNRs) in PK89 and NM01, we also present new results to cover the full parameter space.

The beam combination geometry is a major issue in studying the sensitivity of an interferometer. One extreme is the ${}^nC_2$ interferometer, in which n beams are divided into $n(n-1)$ subbeams and they are pairwise combined at ${}^nC_2 = n(n-1)/2$ detectors. There is one detector for each baseline. The other extreme is the ${}^nC_n$ interferometer in which all the n beams are combined at ${}^nC_n = 1$ detector. In this paper, we present the sensitivities of both interferometers. We consider idealized interferometers, but the beam-combination scenario for actual interferometers

may be more complicated (Mozurkewich (2000)). The ${}^{n}C_2$ and ${}^{n}C_n$ schemes are called Pairwise and All-On-One combinations in Mozurkewich (2000).

Baseline redundancy is a factor that affects the SNR of a synthesis image for a given number of apertures. Since the number of large telescopes combined to form an interferometric array is likely to be limited, it is important to gain uv coverage by using nonredundant baselines. Throughout this paper, we only consider interferometers with nonredundant baselines.

There are two types of noise which appear in aperture synthesis, one of which is removable while the other is intrinsic and not removable. Sampling noise is potentially introduced by the incompleteness of uv coverage. However, deconvolution techniques such as CLEAN and Maximum Entropy Method (MEM) (Perley et al. (1989)), when applied to radio interferometric data, appear to compensate for sampling noise. We thus regard sampling noise as removable noise. On the other hand, noise resulting from the photodetection process is not removable. The SNR of a dirty image to which deconvolution has not been applied is limited by photodetection noise and detector read noise. Here we regard the SNR of a dirty image as the SNR of the synthesized image.

There are two different methods by which a synthesized image can be constructed from the visibility data: inversion without total counts and true inversion. In the former, the zero frequency phasor is neglected, implying that the total number of photons in the synthesized image is zero. Despite this seemingly unattractive feature, this is the standard method in radio astronomy. In the latter method, the van Cittert-Zernike theorem is strictly applied and the zero frequency phasor as well as the $n(n-1)/2$ complex phasors is used. The image produced by this technique has the desirable property of nonnegativity. In the presence of additive background which overwhelms the signal, the magnitude of the zero frequency phasor is much greater than those of other phasors. The zero frequency phasor determines the DC offset level due to thermal background in the synthesized image. Not only is this background of little astronomical interest, it is also a major source of Poisson fluctuations. In this paper, we present the results obtained for both inversion with and without total counts. However, in practice faint source detection is limited by OH airglow background at J and H and thermal background in the thermal infrared. So we obtain those detection limits for inversion without total count.

The paper is organized as follows. First we introduce two types of interferometers, the ${}^{n}C_2$ interferometer and ${}^{n}C_n$ interferometer with expressions for SNRs of the images obtained by these interferometers in §2 and §3. We discuss limiting cases for spectrally broad light in §4. In §5, we present the sensitivities of interferometers composed of nine 10-m telescopes in comparison with a single 30-m telescope with adaptive optics. We discuss further on the sensitivity analysis in §6.

2. ${}^{n}C_2$ interferometer

Let there be n identical principal apertures from which we derive n main beams. Each beam is divided into $n-1$ subbeams by the use of beam splitters. The resulting $n(n-1)$ subbeams are

combined pairwise at $n_b = n(n-1)/2$ detectors where n_b is also the number of baselines. The fringe pattern is formed at the focal plane of each detector which is either a one dimensional array of identical pixels or a two dimensional array of identical pixels which range from 1 to P (Figure 1). For spectrally broad light, the fringe can be dispersed in the cross fringe direction with the use of a two dimensional detector. For a focal plane interferometer of this type, the influence of source shot noise on fringe phasor estimation has been fully formulated (Walkup & Goodman (1973), Goodman (1985)). Let the interferometer be illuminated by a source and spatially smooth background. The intensity pattern on the rth detector (rth baseline) is given by

$$< I_r(\mathbf{x}) >= 2 < I_0 > \Big[1 + \gamma_r \cos(\kappa \mathbf{x} \cdot \mathbf{B}_r/d + \phi_r)\Big], \tag{1}$$

where $< I_0 >$ is the average intensity in each subbeam at the detector, $\mathbf{B}_r$ is the baseline vector, $\kappa = 2\pi/\lambda$ is the wave number, and d is the distance between the aperture plane and the detector, $\mathbf{x}$ is the spatial vector in the detector plane, and $\gamma_r \exp(i\phi_r)$ is the complex visibility function at the baseline vector $\mathbf{B}_r$. In deriving (1), we have assumed that the incident light is spectrally narrow so that the fringe visibility depends on only the spatial correlation of the field.

Because of the presence of background illumination,

$$I_0 = I_0^s + I_0^b, \tag{2}$$

where I_0^s and I_0^b are source and background intensities respectively. Let γ_r^s be the fringe visibility of the source in the absence of the background, then

$$\gamma_r = \frac{I_0^s}{I_0^s + I_0^b}\gamma_r^s. \tag{3}$$

The complex visibility function $\gamma_r^s \exp(i\phi_r)$ is determined by the uv coordinates of the r th baseline (u, v) and the source brightness distribution on the sky $S(x, y)$ by a Fourier transform relation:

$$\gamma_r^s \exp(i\phi_r) = \frac{\int S(x, y) \exp\{-2\pi i(ux + vy)\} dxdy}{\int S(x, y) dxdy}. \tag{4}$$

In an effort to reduce the clutter in the equations we henceforth drop the vector notation, but bear in mind that spatial frequencies, pixel locations, etc. are really vectors. The photoelectron detection theory (Walkup & Goodman (1973)) takes into account the discrete nature of both photons and detector pixels. The average photoelectron count $< k_r(p) >$ at the pixel location specified by the integer index p of the detector is proportional to $< I(x) >$:

$$< k_r(p) >= 2 < K_0 > \Big[1 + \gamma_r \cos(p\omega_r + \phi_r)\Big]. \tag{5}$$

Here, $< ... >$ denotes averaging over the photoelectron-detection process. The product $p\omega_r$ is understood to be the scalar product of the pixel position vector $\mathbf{p}$ and the spatial frequency vector ω_r expressed in inverse pixel units.

Let $< C >$ be the average number of photoelectrons detected by the entire array in one integration period, and let $2< N >$ be the average number of photoelectrons per detector per integration time. Clearly then, $< C >= 2 < N > n_b$, and thus $< N >=< C > /\{n(n-1)\}$. According to (5), the average number of photoelectrons per detector is equal to $2 < K_0 > P$, and thus $< K_0 > P =< N >$.

2.1. Inversion without total count

An analysis based on the photodetection theory gives the mean image I_1 as follows (NM01).

$$\begin{aligned} I_1(q) &= < N > \sum_r \gamma_r \cos(\omega_r q + \phi_r) \\ &= < N > \sum_r \frac{I_0^s}{I_0^s + I_0^b} \gamma_r^s \cos(\omega_r q + \phi_r), \end{aligned} \tag{6}$$

where q refers to the pixels in the synthesized image; in particular q ranges from -Q/2 to +Q/2.

The variance $V[i_1(q)]$ in the synthesized image $i_1(q)$ is given by

$$V[i_1(q)] = n_b(< N > + \frac{P\sigma^2}{2}) = \frac{< C >}{2} + n_b \frac{P\sigma^2}{2}. \tag{7}$$

For a point source ($\gamma_r^s = 1$) at the phase center ($\phi_r = 0$), the SNR of the synthesized image is

$$\frac{I_1(0)}{\sqrt{V[i_1(0)]}} = \frac{(< C > /2)\{I_0^s/(I_0^s + I_0^b)\}}{\sqrt{< C > /2 + n_b P\sigma^2/2}}. \tag{8}$$

2.2. Inversion with total count

An analysis which takes into account shot noise and detector read noise gives the mean image I_2 as follows

$$I_2(q) = < N > \sum_r [\gamma_r \cos(\omega_r q + \phi_r) + 1]$$

$$= \; < N > \sum_r [\frac{I_0^s}{I_0^s + I_0^b} \gamma_r^s \cos(\omega_r q + \phi_r) + 1]. \tag{9}$$

The variance $V[i_2(q)]$ in the synthesized image $i_2(q)$ is given by

$$\begin{aligned} V[i_2(q)] &= n_b(\frac{3 < N >}{2} + \frac{3P\sigma^2}{4}) + < N > \sum_r \gamma_r \cos(\omega_r q + \phi_r) \\ &= \frac{3 < C >}{4} + n_b \frac{3P\sigma^2}{4} + < N > \sum_r \gamma_r \cos(\omega_r q + \phi_r). \end{aligned} \tag{10}$$

This variance is newly derived for this work. For a point source at the phase center, the SNR of the image is

$$\frac{I_2(0)}{\sqrt{V[i_2(0)]}} = \frac{< N > \sqrt{n_b}(2I_0^s + I_0^b)/(I_0^s + I_0^b)}{\sqrt{(3 < N > /2 + 3P\sigma^2/4) + < N > I_0^s/(I_0^s + I_0^b)}} \tag{11}$$

3. ${}^nC_n$ Interferometer

In the ${}^nC_n$ interferometer, all the n beams interfere on a single detector and n_b fringes are superposed. Both the baseline configuration and the detector can be either one dimensional or two dimensional. As an example, a two dimensional ${}^3C_3$ interferometer is schematically presented in Figure 2. A special case is the combination of a one dimensional baseline configuration and a two dimensional detector for which the superposed fringes are dispersed in the cross fringe direction so that spectrally broad light can be used without bandwidth smearing (Figure 3). We call an ${}^nC_n$ interferometer of this type an ${}^nC'_n$ interferometer.

Let the interferometer be composed of n identical apertures and let it be illuminated by a source and spatially smooth background. The classical intensity distribution of the interference pattern by the n apertures has the average value

$$< I(\mathbf{x}) > = < I_0 > \Big[n + 2 \sum_{g<h} \gamma_{gh} \cos(\kappa \mathbf{x} \cdot \mathbf{B}_{gh}/d + \phi_{gh}) \Big], \tag{12}$$

where the various symbols have meanings similar to those in (1). gh denotes the baseline gh corresponding to the apertures g and h. Let $< k(\mathbf{p}) >$ denote the photoelectron count distribution due to $< I(\mathbf{x}) >$. As in §2, we discontinue the vector notation, assume that the total number of pixels is P, and note that $< k(p) >$ is proportional to $< I(x) >$:

$$< k(p) > = < Q_0 > \Big[n + \sum_{g<h} \gamma_{gh} \cos(p\omega_{gh} + \phi_{gh}) \Big]. \tag{13}$$

Here $< Q_0 >$ has approximately the same meaning as $< K_0 >$ in §2. However, since there is no beam splitting, $< Q_0 >= (n-1) < K_0 >$. We also define $< M >= P < Q_0 >=< C > /n$.

3.1. Inversion without total count

We find the mean synthesized image I_3 to be

$$I_3(q) \quad = \quad < M > \sum_{i<j} \gamma_{ij} \cos(q\omega_{ij} + \phi_{ij}). \tag{14}$$

The variance $V[i_3(q)]$ in the synthesized image $i_3(q)$ is given by

$$V[i_3(q)] \quad = \quad \frac{n < M > +P\sigma^2}{2} n_b + < M > (n-2) \sum_{i<j} \frac{I_0^s}{I_0^s + I_0^b} \gamma_{ij}^s \cos(q\omega_{ij} + \phi_{ij}). \tag{15}$$

This variance is derived in NM01. For a point source at the phase center, the SNR of the image is

$$\begin{aligned} \frac{I_3(0)}{\sqrt{V[i_3(0)]}} &= \frac{< M > \{I_0^s/(I_0^s + I_0^b)\}\sqrt{n_b}}{\sqrt{(n < M > +P\sigma^2)/2 + < M > (n-2)\{I_0^s/(I_0^s + I_0^b)\}}} \\ &= \frac{< C > \{I_0^s/(I_0^s + I_0^b)\}\sqrt{(n-1)/n}}{\sqrt{< C > +P\sigma^2 + < C > \{I_0^s/(I_0^s + I_0^b)\}\{2(n-2)/n\}}}. \end{aligned} \tag{16}$$

3.2. Inversion with total count

We find the mean synthesized image I_4 to be

$$I_4(q) \quad = \quad < M > [\frac{n}{2} + \sum_{i<j} \gamma_{ij} \cos(q\omega_{ij} + \phi_{ij})] \tag{17}$$

$$= \quad \frac{< C >}{2} + \frac{< C >}{n} \sum_{i<j} \gamma_{ij} \cos(q\omega_{ij} + \phi_{ij}). \tag{18}$$

The variance $V[i_4(q)]$ in the synthesized image $i_4(q)$ is given by

$$V[i_4(q)] = \frac{<M>}{2}\left[n(n_b+\frac{1}{2}) + 2(n-1)\sum_{i<j} 2(j-1)\gamma_{ij}\cos(q\omega_{ij}+\phi_{ij})\right] \quad (19)$$

$$+P\sigma^2\left[\frac{n_b}{2}+\frac{1}{4}\right]. \quad (20)$$

This variance is newly derived for this work. For a point source at the phase center, the SNR of the image is

$$\frac{I_4(0)}{\sqrt{V_4(0)}} = \frac{<C>n}{\sqrt{<C>(3n^2-5n+3)+P\sigma^2(n^2-n+1)}}. \quad (21)$$

4. Limiting Cases for Spectrally Broad Light

In this section, we consider the source shot noise limit, background shot noise limit, and detector read noise limit for a point source and an extended source. For each case, the results of inversion with and without total count are shown.

Formulae for means, variances, and SNRs were obtained for spectrally narrow light in the previous section. For a two-dimensional ${}^nC_n$ interferometer, the maximum spectral bandwidth is limited to about D/B where D is the aperture diameter and B is the maximum baseline length. If we use a bandwidth broader than this, fringes will be smeared out. In order to disperse fringes for a general two-dimensional baseline configuration, pupil remapping which transforms the exit pupil to a ${}^nC'_n$-type interferometer is necessary. The effect of pupil remapping on the signal-to-noise ratio analysis is beyond the scope of this paper. However we can imagine that the SNR of the one-dimensional ${}^nC'_n$ interferometer is a good measure of the SNR of an interferometer with pupil remapping. For ${}^nC_2$ and ${}^nC'_n$ interferometers, fringes can be dispersed in the cross fringe direction. The formulae for SNRs obtained for spectrally narrow light hold also for dispersed fringes as can be easily verified as follows.

We here consider the case with the ${}^nC_2$ interferometer and inversion without total count. Let P_x be the number of pixels in the fringe direction and P_y be that in the cross fringe direction. Therefore $P = P_xP_y$. We assume that the photon spectrum within the bandwidth is not steep and the number of photons in one detector row is given by $<C>/P_y$. Then the SNR of an image synthesized from a set of fringes in detector rows corresponding to $1/P_y$ of the spectral bandwidth is given by

$$snr = \frac{<N>/P_y\sum_r\gamma_r\cos(\omega_r q+\phi_r)}{\sqrt{n_b(<N>/P_y+P_x\sigma^2/2)}}. \quad (22)$$

If we further assume that the total bandwidth is narrow enough so that the source structure does not change within it. In this case, P_y images can be coadded to form a final image. The SNR of the final image is given by

$$\begin{aligned} SNR &= \sqrt{P_y} snr \\ &= \frac{< N > \sum_r \gamma_r \cos(\omega_r q + \phi_r)}{\sqrt{n_b(< N > + P_x P_y \sigma^2/2)}} \\ &= \frac{< N > \sum_r \gamma_r \cos(\omega_r q + \phi_r)}{\sqrt{n_b(< N > + P\sigma^2/2)}}. \end{aligned} \tag{23}$$

This happens because the photon count $< N >$ or $< C >$ and the pixel number P are linear in the expressions of the mean and variance. The situation is the same for the other SNR expressions.

4.1. Numbers of Pixels

Let the central frequency be ν and the bandwidth be $\Delta\nu$. Then there are $2\nu/\Delta\nu$ fringe cycles in each interferogram. For the Nyquist sampling theorem, $4\nu/\Delta\nu$ pixels are needed in the fringe direction.

For the ${}^nC_2$ and ${}^nC'_n$ interferometers, we consider the number of pixels in the cross fringe direction (dispersion direction) in each dispersed fringe. The fractional bandwidth $\Delta\nu^*/\nu$ for which bandwidth smearing is small is given by $\Delta\nu^*/\nu < D/B$. If we require that $\Delta\nu^*/\nu = D/(2B)$, bandwidth smearing will be negligible. For a spectral bandwidth of $\Delta\nu$, $\Delta\nu/\Delta^*\nu = 2(\Delta\nu)/(D/B)$ pixels are needed as the number of pixels in the cross fringe direction. So the number of pixels of the two dimensional detector is $P = 4\nu/\Delta\nu \times 2(\Delta\nu)/(D/B) = 8(B/D)$.

For the ${}^nC_n$ interferometer, the longest baseline can be aligned to one of the two sides of a two dimensional detector and the minimum number of pixels is $P = (4\nu/\Delta\nu)^2 = 16(B/D)^2$ and the maximum allowed fractional bandwidth is D/B.

4.2. SNR Tables

SNR expressions of ${}^nC_2$, ${}^nC_n$, and ${}^nC'_n$ interferometers are given for a point source and an extended source, for source shot noise limit, background shot noise limit, and detector read noise limit, and for inversion with and without total count in Tables 1 through 5. In some cases the SNR expressions are not well defined and omitted from the tables.

We define a quantity F_ν which is proportional to the photon spectrum of the source, collecting

area, and integration time. We express the total photon count for the ${}^nC_2$ and ${}^nC'_n$ interferometers as $< C >= F_\nu \Delta\nu$. Then the total photon count for the two-dimensional ${}^nC_n$ interferometer is $< C >= F_\nu \nu(D/B)$. The SNRs are expressed in terms of F_ν, $\Delta\nu$, and D/B.

4.3. Point Source/Source Shot Noise Limit

The case with a point source in the shot noise limit is given in Table 1.

By taking ratios of the SNR expressions, we find

$$SNR_1/SNR_3 = \sqrt{\frac{3n-4}{2n-2}}\sqrt{\frac{\Delta\nu/\nu}{D/B}}, \tag{24}$$

$$SNR_1/SNR'_3 = \sqrt{\frac{3n-4}{2n-2}} \geq 1, \tag{25}$$

$$SNR_2/SNR_4 = \sqrt{\frac{4(3n^2-5n+3)}{5n^2}}\sqrt{\frac{\Delta\nu/\nu}{D/B}}, \tag{26}$$

$$SNR_2/SNR'_4 = \sqrt{\frac{4(3n^2-5n+3)}{5n^2}} \geq 1, \tag{27}$$

$$SNR_2/SNR_1 = \sqrt{\frac{8}{5}}. \tag{28}$$

In a typical situation, $\Delta\nu/\nu > D/B$ and the ${}^nC_2$ and ${}^nC'_n$ interferometers are superior to the two-dimensional ${}^nC_n$ interferometer. As the expression (27) shows, the ${}^nC_2$ interferometer is superior to the ${}^nC'_2$ interferometer by a factor $\sqrt{12/5}$ in SNR for a large n for inversion with total count. In the source shot noise limit, the total count information is genuinely of the source. The highest SNR is obtained for the ${}^nC_2$ interferometer for inversion with total count (eq. (28)).

4.4. Background Limit

In the background limit, only inversion without total count is the valid method of analysis, since the total count is dominated by background photon counts. The SNR expressions are given in Table 2.

By taking the ratios, we find

$$SNR_1/SNR_3 = \sqrt{\frac{n}{2(n-1)}}\sqrt{\frac{\Delta\nu/\nu}{D/B}}, \tag{29}$$

and

$$SNR_1/SNR_3' = \sqrt{\frac{n}{2(n-1)}} \leq 1. \tag{30}$$

As in the case with the source shot noise limit, the two-dimensional ${}^nC_n$ interferometer has a disadvantage of the narrow bandwidth. For a large n, the ${}^nC_n'$ interferometer is slightly superior to the ${}^nC_2$ interferometer by a factor $\sqrt{2}$ in SNR.

4.5. Read noise limit

In the read noise limit, the numbers of pixels for the ${}^nC_2$ and ${}^nC_n'$ interferometers are $P = 8(B/D)$ and that for the two-dimensional ${}^nC_n$ interferometer is $P = 16(B/D)^2$. The SNR expressions are given in Table 3.

If we take the ratios of the SNRs, we find

$$SNR_1/SNR_3 = \frac{\sqrt{2}}{n-1}\frac{\Delta\nu}{\nu}(\frac{B}{D})^{3/2}, \tag{31}$$

$$SNR_1/SNR_3' = \frac{1}{n-1} \leq 1, \tag{32}$$

$$SNR_2/SNR_4 = \frac{4}{n}\sqrt{\frac{n^2-n+1}{3(n^2-n)}}\frac{\Delta\nu}{\nu}(\frac{B}{D})^{3/2}, \tag{33}$$

$$SNR_2/SNR_4' = \frac{2}{n}\sqrt{\frac{2(n^2-n+1)}{3(n^2-n)}} \leq 1. \tag{34}$$

The ${}^nC_n'$ interferometer is always superior to the ${}^nC_2$ interferometer because of the smaller number of detector pixels. The two-dimensional ${}^nC_n$ interferometer has a limited use for a small B/D.

4.6. Extended Source/Source Shot Noise Limit

For a fully extended source, there is no signal other than the total count. Only inversion with total count is the valid method of analysis for the fully extended source. The SNR expressions are given in Table 4.

By taking the ratios, we find

$$SNR_2/SNR_4 = \sqrt{\frac{n^2 - n + 1}{3}} \sqrt{\frac{\Delta\nu}{\nu} \frac{B}{D}}, \tag{35}$$

$$SNR_2/SNR_4' = \sqrt{\frac{n^2 - n + 1}{3}} \geq 1. \tag{36}$$

The ${}^nC_2$ interferometer is superior to the ${}^nC_n$ and ${}^nC_n'$ interferometers.

4.7. Extended Source/Background Limit

For an extended source, there is no signal other than the source total count. However, the total count is dominated by background photons. Therefore neither inversion without total count nor inversion with total count is the valid method of analysis.

4.8. Extended Source/Read Noise Limit

As in the case with extended source/shot noise limit, the only valid method of analysis is inversion with total count. The SNR expressions are given in Table 5.

By taking ratios, we find

$$SNR_2/SNR_4 = \sqrt{\frac{4(n^2 - n + 1)}{3(n^2 - n)} \frac{\Delta\nu}{\nu} (\frac{B}{D})^{3/2}}, \tag{37}$$

and

$$SNR_2/SNR_4' = \sqrt{\frac{2(n^2 - n + 1)}{3(n^2 - n)}} \leq 1. \tag{38}$$

The two-dimensional ${}^nC_n$ interferometer is useful only for a small B/D. For large n, SNR_2/SNR_4' attains an asymptotic value of $\sqrt{2/3}$.

5. Sensitivities of Interferometers Composed of Nine 10-m telescopes

In this section, we calculate the sensitivities of ${}^nC_2$ and ${}^nC'_n$ interferometers composed of nine 10-m telescopes and compare them with the sensitivity of a 30-m single telescope with adaptive optics. 10-σ detection limits for a point source are obtained for one-hour integration and plotted in Figure 4.

5.1. J and H

Throughput of the interferometers is assumed to be 10%, while that of the single telescope with adaptive optics is assumed to be 60%. The read noise level is assumed to be 10 electrons per pixel and the maximum baseline length which determines the number of detector pixels is assumed to be 200 m. The coherent integration time is assumed to be one second, while a larger value will decrease the effect of detector read noise.

It turned out that both read noise and sky background due to OH airglow affect the performance of the interferometers. We evaluate the SNRs for inversion without total count because sky background is much greater than the signal near the detection limit. The sensitivity of the telescope is limited by sky background. At J, limiting magnitudes are 24.7, 25.7, and 28.0 respectivity for the ${}^nC_2$ interferometer, ${}^nC'_n$ interferometer, and the single telescope. At H, they are 23.6, 24.0, and 26.2 respectively.

5.2. Thermal Infrared Wavelengths

For the interferometers, we evaluate the SNRs for inversion without total count because the instrument background is much stronger than the source signal near the detection limits. The temperature of interferometer optics is assumed to be 273 K and the optical throughput is assumed to be 10%. Therefore the background emission is estimated from a 273K blackbody with 90% emissivity. For the single telescope with adaptive optics, the throughput of the optics is assumed to be 60%. The temperature of the optics is assumed to be 273 K, and its emissivity is assumed to be 40%.

Longward of 2 μm, the sensitivities do not depend on beam combination geometry very much. This implies that detector read noise is negligible. At 2.2 μm, the sensitivities of the interferometers are around 330 nJy or 22.9 mag, while that of the single telescope is 10 nJy or 26.9 mag. Longward of 5 μm, the single telescope is 5.8 mag more sensitive than the interferometers. At 10.5 μm, the sensitivities of the interferometers are about 2 mJy or 10.7 mag, while that of the single telescope is 57 μJy or 14.4 mag. At wavelengths shorter than 2 μm, the baseline length affects the sensitivities of the interferometers due to the change in the number of pixels, while longward of 2 μm, it does not matter as long as the source is unresolved. Here we do not

consider the case for a fully extended objects. As we have seen from the previous section, the interferometers are not sensitive to fully extended objects under background limited conditions.

5.3. Loss-Free Interferometers

In the above evaluation of sensitivities, it is assumed that the throughput of the interferometers is 10%, while that of the single telescope is 60%. It is natural to question whether the difference in sensitivities is due to that in throughput or something more fundamental.

As discussed by PK89, there is a basic difference between an interferometer and a single telescope in that the former takes the correlation of signal from multiple apertures. However the loss of SNR by this process is only a factor of $\sqrt{2}$ in the case of an ideal ${}^{n}C_2$ interferometer with inversion without total count in the source shot noise limit. A similar situation is expected in the case of background shot noise limit where the number of detector pixels does not affect the SNR. Then the only situation in which the difference is conspicuous is the read noise limit where the interferometer requires many more detector pixels to sample fringes. It is of theoretical interest to assume ideal interferometers and compare their performance with that of the single telescope.

Again we compare the interferometers with nine 10-m telescopes and a 30-m single telescope. Since each of the 10-m telescope and the 30-m single telescope require adaptive optics, the throughputs are assumed to be 60%. The sensitivity limits are plotted in Figure 5, where the difference is about by a factor of five. Therefore the fundamental difference between in the interferometers and the single telescope is rather small and the large difference seen in the previous analysis is due to that in throughput.

5.4. Baseline Dependence

The SNR expressions of the interferometers are not explicitly baseline dependent. Since the astronomical source is assumed to be unresolved, only the total number of detector pixels is dependent on the lengths of baselines. Detector read noise is more significant as the baselines become longer. In order to use long baselines, it is essential to keep detector read noise low so that the SNR is not limited by read noise.

For a source of finite extent, long baselines start to resolve it and the visibilities γ_r^s of those baselines decrease from unity and the phases ϕ_r become less coherent depending on the symmetry of the source. For the extended source, the SNRs of the interferometers are calculated as follows. For a particular baseline configuration, the complex visibilities are obtained by the Fourier transform relation (4) and the number of detector pixels are calculated as above. By inserting those numbers and taking the summation over different baselines, one can obtain the SNRs of the dirty images.

6. Discussion

6.1. Interferometry for extragalactic astronomy

One of the motivations of this analysis is to evaluate the capability of interferometry for extragalactic astronomy. We inevitably have to consider extended objects for this purpose and take into account the guide star availability. Fringe tracking requires the presence of a natural guide star in the infrared. If the adaptive optics also needs the same natural guide star, the limiting magitude is around R = 15, and an isoplanatic angle is order of $10''$ at 2 μm. Requirements for a natural guide star limit the range of observing targets to bright active galactic nuclei (AGNs) and bright quasars.

The central continuum source of an AGN or a quasar will act as a natural guide star and the fringe visibilities are close to unity and phases are close to zero. Therefore SNR calculations made in the previous section are applicable to this case. Small deviations in a reconstructed image from a point source indicate the presence of a faint extended structure such as jet. The 10σ limiting magnitude of K=25 indicates SNR = 10^5 for a K=15 quasar. In other words, jet can be searched for with a dynamic range of 10^5:1.

Now we consider resolving broad-line regions (BLRs). According to the photoionization model (Davidson & Netzer (1979)), the size of a BLR scales as $\sqrt{L}$ where L is the luminosity of the AGN. For an AGN or a nearby quasar toward which the geometry is Euclidean, the observed flux f is given by $f = L/d^2$ where d is the distance to the object. Then the angular size $\theta \propto \sqrt{f}$. Therefore the brightest quasar has the largest BLR in angular size. 3C273 is the brightest quasar (K=10) and easiest to observe because Paα is redshifted to K band. The necessary spatial resolution is order of 1 milliarcsecond or the necessary baseline length is 400 m. The FWHM of the line is 3400 kms^{-1} and the line/continuum ratio below 8000 kms^{-1} is 0.08 (Sellgren et al. (1983)). In order to obtain the spatial structure of the BLR, we wish to spectrally resolve the broad line or at least separate the blue and red components. If we require a spectral resolution of 3000 kms^{-1}, the continuum flux per spectral resolution is K=14 equivalent. A spectral image will be composed of an unresolved source of K=14 and a resolved source with 8% of the flux of the unresolved source. Again, the complex visibilities are close to those of a point source and the SNR argument made above for jet applies to this case as well. We expect that the BLR of 3C273 will be resolved with a dynamic range more than 10^5:1. At least for AGNs and quasars, infrared interferometry with large telescopes appears effective.

6.2. Comments on RR99

In this subsection, we compare our results with that of RR99 on Fizeau-type interferometers or two-dimensional ${}^nC_n$ interferometers. First of all, for spectrally broad light, we have seen that two-dimensional ${}^nC_n$ interferometers or Fizeau-type interferometers have limitations in the ratio

of the telescope aperture diameter and the baseline length to avoid bandwidth smearing. This is not discussed in RR99. Second, RR99 states that the ${}^{n}C_{n}$ interferometer is superior to the ${}^{n}C_{2}$ interferometer. However, we have seen from the analysis of limiting cases that the situation is not so simple. As PK89 noted, there is no major difference in performance between both interferometers in the source shot noise limit. This is also true with the case for the background limit. In the read noise limit, the ${}^{n}C_{n}'$ interferometer is superior to the ${}^{n}C_{2}$ interferometer due to the difference in the number of detector pixels.

These differences originates from that in the definitions of the SNRs. RR99 defines the SNR as that of the central peak in the interferogram directly formed by beam combination. On the other hand, we define the SNR as that of the dirty image formed by aperture synthesis. In the latter, the interferogram formed by beam combination is Fourier transformed to measure complex visibilities which fill the uv plane and then they are Fourier transformed back to the image plane to form a dirty image. In RR99, the detector pixels of concern at the focal plane are only a few pixels at which the peak is located, while in the latter many pixels which sample the entire interferogram are considered.

6.3. Remaining Issues

We have obtained the sensitivity limits of the interferometers for perfect wavefront correction by adaptive optics and perfect fringe tracking. In reality, both adaptive optics and fringe tracking require a guide star and there is a limitation in the precision of wavefront and delay compensations. Imperfection in phase directly influences the fringe visibility γ which is proportional to the SNRs. An analysis which takes into account this imperfection in phase is difficult because introduction of atmospheric disturbances opens up a vast parameter space. Our analysis corresponds only to the best case designing.

In this paper, we considered only nonredundant baselines. However, if we consider a closely packed array of telescopes, we have to take into account the redundancy of the baselines. Although the behavior of SNRs are expected to be the same as the nonredundant case, deriving formulae of SNRs for the redundant case is non trivial or analytically impossible.

Finally one essential and difficult question is whether the definition of the SNR as that of the dirty image is valid. In other words, we have left out the issue of deconvolution by assuming that it is perfect. We believe that this is practically of no problem because the SNR of the dirty beam is usually much higher than that of the dirty image. Nevertheless deconvolution is a nonlinear process and the error propagation through it is not fully understood.

7. Conclusions

We present the formulae of SNRs of interferometers for the purpose of comparing ground-based interferometers composed of multiple large telescopes with a single giant telescope with adaptive optics. In deriving sensitivity limits, perfect wavefront correction by adaptive optics and perfect cophasing by fringe tracking are assumed. We consider the case in which n beams are pairwise combined at $n(n-1)/2$ detectors (${}^nC_2$ interferometer) and the case in which all the n beams are combined at a single detector (${}^nC_n$ interferometer).

(1) In the read noise limit, the ${}^nC_n$ interferometer with one dimensional baseline configuration is superior to the ${}^nC_2$ interferometer, while in the background limit, the advantage of the ${}^nC_n$ interferometer is small.

(2) We compare the point-source sensitivities of interferometers composed of nine 10-m diameter telescopes and a 30-m diameter single telescope with adaptive optics between 1 and 10 μm for 10-σ detection in one hour. Between 1 and 2 μm, the sensitivities of the interferometers are limited by detector read noise and sky background, while longward of 2 μm, they are limited by the instrumental thermal background. At K band, the sensitivities of the interferometers are around 23 mag, while that of the single telescope is 27 mag.

I thank H. Matsuhara for allowing me to use figures and the referee P. Lawson for useful comments.

REFERENCES

Davidson, K. and Netzer, H. 1979, Rev. Mod. Phys. 51, 715

Goodman, J. W. 1985, Statistical Optics, Wiley, NY

Mozurkewich, D. 2000, Chap 14 of "Principles of Long Baseline Interferometry" Course Notes from 1999 Michelson Summer School, Lawson, P. Ed. JPL Publication 00-009 07/00 (http://sim.jpl.nasa.gov/library/coursenotes.html)

Nakajima, T., and Matsuhara, H. 2001, Appl. Opt. 40, 514

Perley, R. A., Schwab, F. R., Bridle, A. H. 1989, Synthesis Imaging in Radio Astronomy, NRAO Workshop No. 21, ASP Conference Series, San Francisco

Prasad, S. and Kulkarni, S. R. 1989, J. Opt. Soc. Am. A6, 1702

Roddier, F., and Ridgway, S. T. 1999, PASP, 111, 990

Sellgren, K., Soifer B. T., Neugebauer, G. and Matthews, K. 1983, PASP, 95, 289

Walkup, J. F. and Goodman, J. W. 1973, J. Opt. Soc. Am, 63, 399

This preprint was prepared with the AAS LaTeX macros v4.0.

Fig. 1.— Schematic diagram of a focal plane interferometer. There is one detector for each baseline.

Fig. 2.— Schematic diagram of a ${}^3C_3$ interferometer. Beams from all apertures are superposed on a single detector.

Fig. 3.— Schematic diagram of a one-dimensional ${}^3C_3$ interferometer. Fringes are spectrally dispersed in cross fringe direction.

Fig. 4.— Detection limits of the ${}^nC_2$- and 1D ${}^nC_n$ interferometers and that of the single giant telescope are plotted as functions of wavelength. Symbols are sensitivities are at J and H of ${}^nC_2$ (asterisk), 1D ${}^nC_n$ (square) and telescope (circle). Assumed parameters are described in the text.

Fig. 5.— Loss-Free Interferometers. Throughputs of the interferometers and the single telescope are assumed to be the same. Meanings of the symbols are the same as in Figure 4.

Table 1. SNR (Point Source / Shot Noise Limit)

Case	Notation	Expression
${}^nC_2$/inversion w/out total count	SNR_1	$\sqrt{\frac{F_\nu \Delta\nu}{2}}$
${}^nC_2$/inversion with total count	SNR_2	$\sqrt{\frac{4}{5}}\sqrt{F_\nu \Delta\nu}$
${}^nC_n$/inversion w/out total count	SNR_3	$\sqrt{\frac{n-1}{3n-4}}\sqrt{F_\nu \nu \frac{D}{B}}$
${}^nC_n$/inversion with total count	SNR_4	$\sqrt{\frac{n^2}{3n^2-5n+3}}\sqrt{F_\nu \nu \frac{D}{B}}$
${}^nC'_n$/inversion w/out total count	SNR'_3	$\sqrt{\frac{n-1}{3n-4}}\sqrt{F_\nu \Delta\nu}$
${}^nC'_n$/inversion with total count	SNR'_4	$\sqrt{\frac{n^2}{3n^2-5n+3}}\sqrt{F_\nu \Delta\nu}$

Table 2. SNR (Point Source / Background Limit)

Case	Notation	Expression
${}^nC_2$/inversion w/out total count	SNR_1	$\frac{I_0^s}{I_0^b}\sqrt{\frac{F_\nu \Delta\nu}{2}}$
${}^nC_n$/inversion w/out total count	SNR_3	$\frac{I_0^s}{I_0^b}\sqrt{\frac{n-1}{n}}\sqrt{F_\nu \nu \frac{D}{B}}$
${}^nC'_n$/inversion w/out total count	SNR'_3	$\frac{I_0^s}{I_0^b}\sqrt{\frac{n-1}{n}}\sqrt{F_\nu \Delta\nu}$

Table 3. SNR (Point Source / Read Noise Limit)

Case	Notation	Expression
${}^nC_2$/inversion w/out total count	SNR_1	$\frac{1}{4\sqrt{n_b(B/D)}}\frac{F_\nu \Delta\nu}{\sigma}$
${}^nC_2$/inversion with total count	SNR_2	$\frac{1}{\sqrt{6n_b(B/D)}}\frac{F_\nu \Delta\nu}{\sigma}$
${}^nC_n$/inversion w/out total count	SNR_3	$\frac{1}{4}\sqrt{\frac{n-1}{n}}(\frac{D}{B})^2\frac{F_\nu \nu}{\sigma}$
${}^nC_n$/inversion with total count	SNR_4	$\frac{1}{4}\sqrt{\frac{n^2}{n^2-n+1}}(\frac{D}{B})^2\frac{F_\nu \nu}{\sigma}$
${}^nC'_n$/inversion w/out total count	SNR'_3	$\frac{1}{\sqrt{8(B/D)}}\sqrt{\frac{n-1}{n}}\frac{F_\nu \Delta\nu}{\sigma}$
${}^nC'_n$/inversion with total count	SNR'_4	$\frac{1}{\sqrt{8(B/D)}}\sqrt{\frac{n^2}{n^2-n+1}}\frac{F_\nu \Delta\nu}{\sigma}$

Table 4. SNR (Extended Source/Source Shot Noise Limit)

Case	Notation	Expression
${}^nC_2$/inversion with total count	SNR_2	$\sqrt{\frac{F_\nu \Delta\nu}{3}}$
${}^nC_n$/inversion with total count	SNR_4	$\sqrt{\frac{F_\nu \nu (D/B)}{n^2-n+1}}$
${}^nC'_n$/inversion with total count	SNR'_4	$\sqrt{\frac{F_\nu \Delta\nu}{n^2-n+1}}$

Table 5. SNR (Extended Source/Read Noise Limit)

Case	SNR	Expression
${}^nC_2$/inversion with total count	SNR_2	$\frac{1}{\sqrt{12(n^2-n)(B/D)}} \frac{F_\nu \Delta\nu}{\sigma}$
${}^nC_n$/inversion with total count	SNR_4	$\frac{1}{\sqrt{16(n^2-n+1)(B/D)^2}} \frac{F_\nu \nu (B/D)}{\sigma}$
${}^nC'_n$/inversion with total count	SNR'_4	$\frac{1}{\sqrt{8(n^2-n+1)(B/D)}} \frac{F_\nu \Delta\nu}{\sigma}$

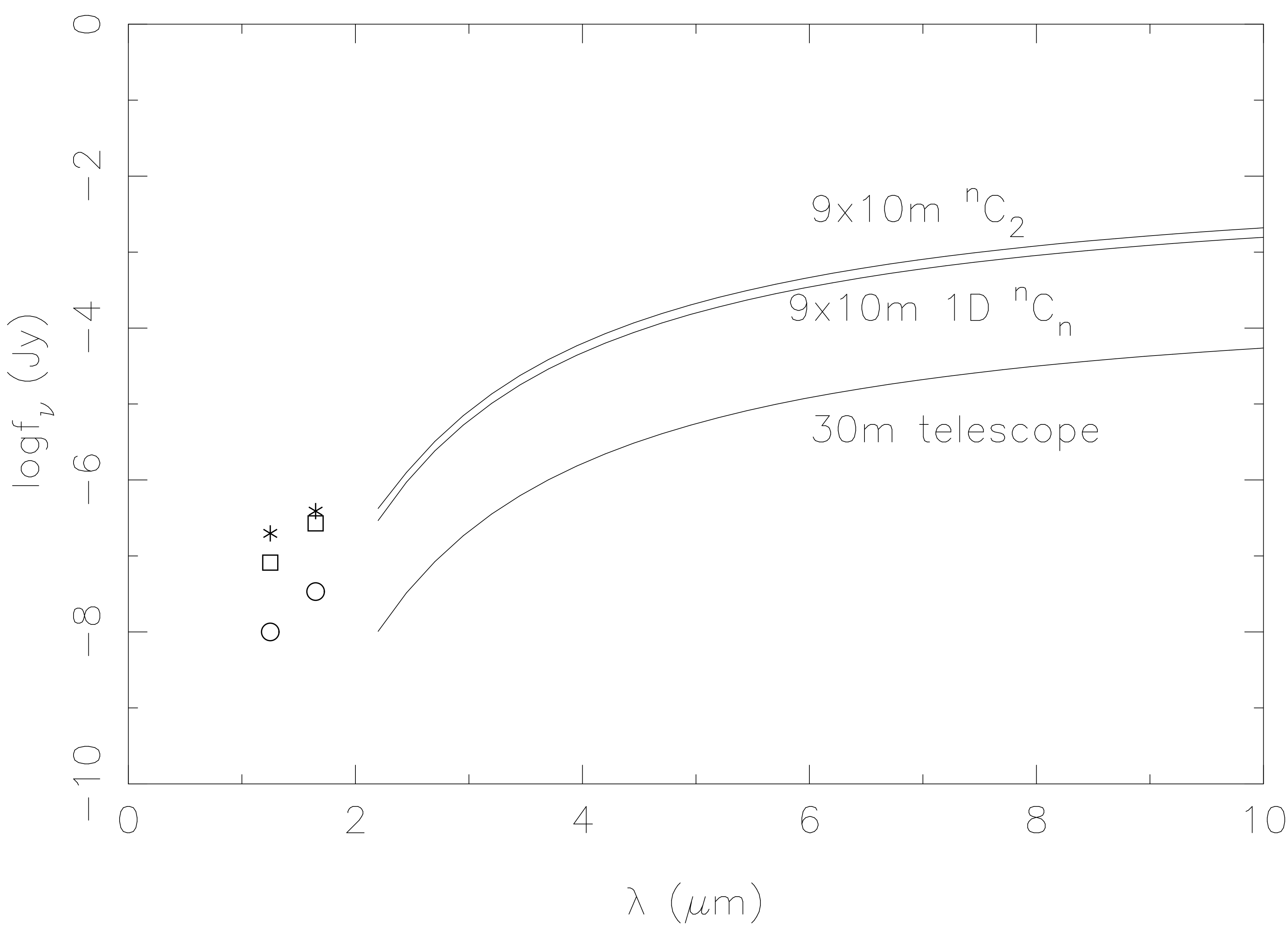
9x10m $^{n}C_{2}$
9x10m 1D $^{n}C_{n}$
30m telescope
$\log f_{\nu}$ (Jy)
λ (μm)
0
−2
−4
−6
−8
−10
0
2
4
6
8
10

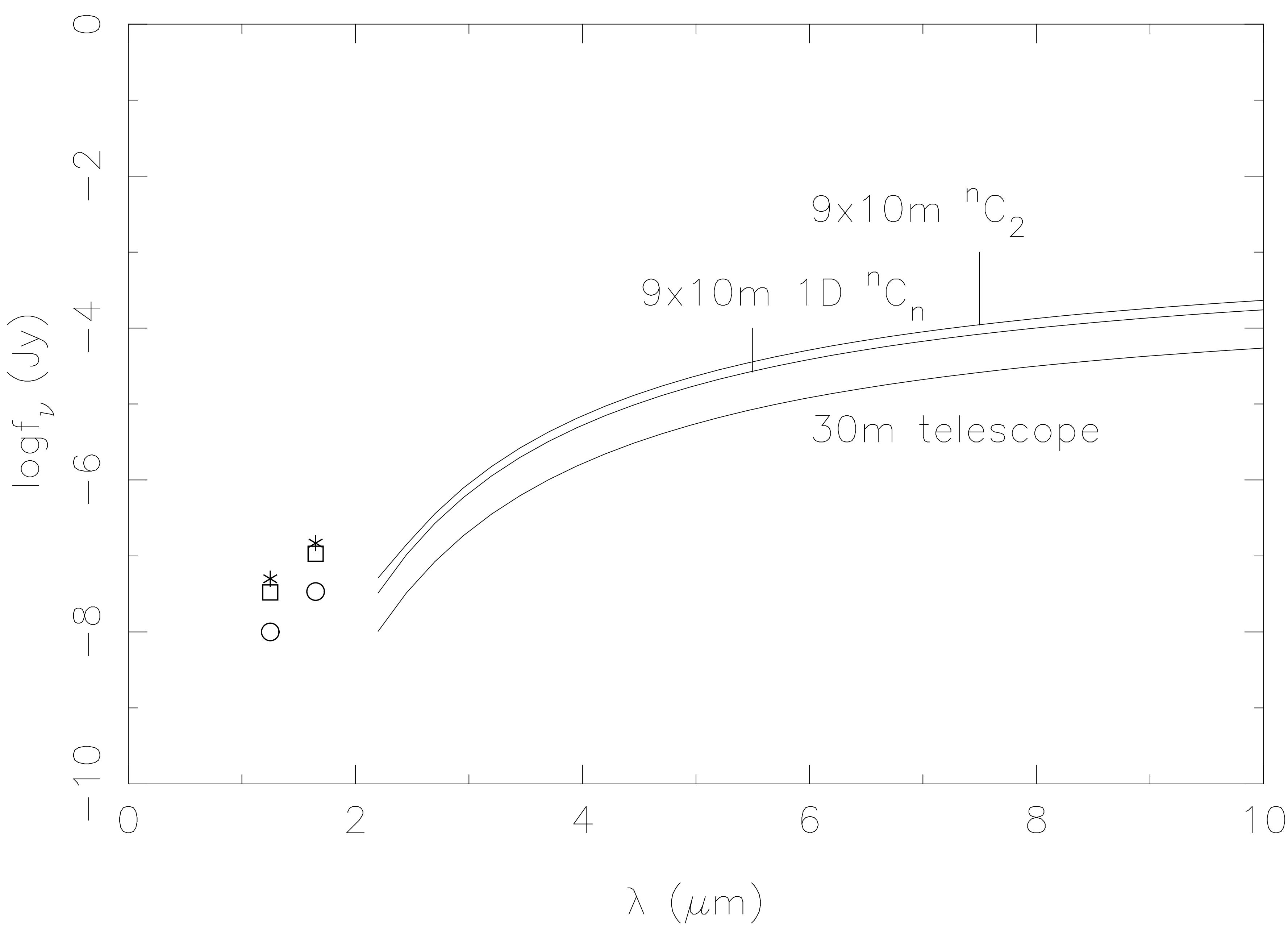

9x10m $^nC_2$
9x10m 1D ^nC_n
30m telescope
0
−2
−4
−6
−8
−10
0
2
4
6
8
10
$\log f_\nu$ (Jy)
λ (μm)